MICROWAVE INTERFEROMETER

By S. K. Chatterjee, (Miss) C. Rama Bai and P. R. Shenoy

(Department of Electrical Communication Engineering, Indian Institute of Science, Bangalore-3)

Received July 20, 1954

Abstract

The design and operation of a two-beam microwave interferometer ($\lambda = 3{\cdot}2$ cm.) using two horns connected to the microwave source by a waveguide is discussed. In order to assess the usefulness of the interferometer, the dielectric constants of some solid insulating materials have been measured. Results obtained using ordinary commercial sheets of materials agree within a few per cent. with values obtained by other methods. The effect of diffraction on phase shift and hence dielectric constant has been investigated. The minimum size of a sample necessary for minimising the effect of diffraction has been determined. The sizes of the sample required for various angles of incidence compared to that at normal incidence have been determined and the results are in agreement with the values obtained theoretically.

The probable error in the measurement of shift for different materials lies between $\pm 0{\cdot}008$ to $\pm 0{\cdot}024$ cm. The value of the dielectric constant measured at normal incidence agrees within $1{\cdot}5\%$ with the value obtained at Brewster's angle after necessary correction.

Description of Apparatus

Microwave interferometers constructed by previous workers (Lengyel, 1949; etc.) work either on the principle of optical interferometers by Michelson, Fabry-Perot or the combination of horn and waveguide. The present interferometer constructed for the purpose of studying the properties of artificial dielectrics at microwave frequencies is essentially a microwave bridge. One arm of the bridge consists of free-space into which the dielectric sample under investigation is inserted. The microwave power is supplied to the bridge from a 723–A/B klystron which is fed from a stabilised power supply unit and modulated with 1000 c.p.s. square wave. The beam divider which is a 20 db. directional coupler placed at the input end of the bridge divides the microwave power into two portions. The main arm of the directional coupler feeds a H-plane sectoral horn, the radiation from which after traversing a portion of the air-gap illuminates the dielectric sample. The second portion of the beam being coupled into the side arm of the directional coupler

travels through a long waveguide, fixed and a precision variable attenuator and reaches one of the side arms of a hybrid junction (magic-tee) which is placed in the output arm of the bridge. The other side arm of the magic-tee is connected through a waveguide and a E-plane bend to a H-plane sectoral horn which is placed in line with the transmitting horn and hence receives the energy transmitted through the sample and through a portion of the air-gap. The two beams travelling through the two side arms of the magic-tee pass in the E-plane arm to a waveguide tuner and finally to a detecting section containing 1N23 crystal. The beams are added algebraically at the crystal, the output of which passes through a co-axial cable to a high gain amplifier. The detector records the energy minima and maxima as the receiving horn is displaced along its axis. The H-plane arm of the hybrid junction is terminated with a matched termination and the E-arm is matched by the waveguide tuner. This avoids interaction between the E and the H-arm. A photograph and a block schematic of the interferometer are shown in Figs. 1 and 2, respectively. Fig. 3 shows the photograph of some of the microwave components constructed for the interferometer.

Phase and Amplitude Balance

The amplitude of the wave travelling through the waveguide path is equalised to that of the wave which has passed through the sample by means of the precision attenuator. The fixed attenuator (20 db.) is placed in order to avoid any interaction between the detector and the source. The phase balance of the bridge is achieved by displacing physically the receiving horn by means of a slow motion driving mechanism. The slow motion drive has been designed in such a way as to restrict the motion of the receiving horn in a straight line coincident with the axis of the transmitting horn. In order to prevent sidewise displacement of the horn during movement, the horn is supported by four sides and two bottom guide rollers fixed in a platform which is provided with four levelling screws. The detector reads energy minima and maxima as the receiving horn is displaced forward and backward. The position of the horn is read with the help of a microscope which can read up to 0·002 cm. One full turn of the slow motion knob gives a movement of the horn of 0·112 cm. The total travel of the receiving horn is 5·0 cm.

Electronic Equipments

The power supply unit for the microwave source consists of a conventional type of stabiliser system. The modulator unit consisting of a multivibrator and amplifier supplies 1000 c.p.s. square wave to the reflector of

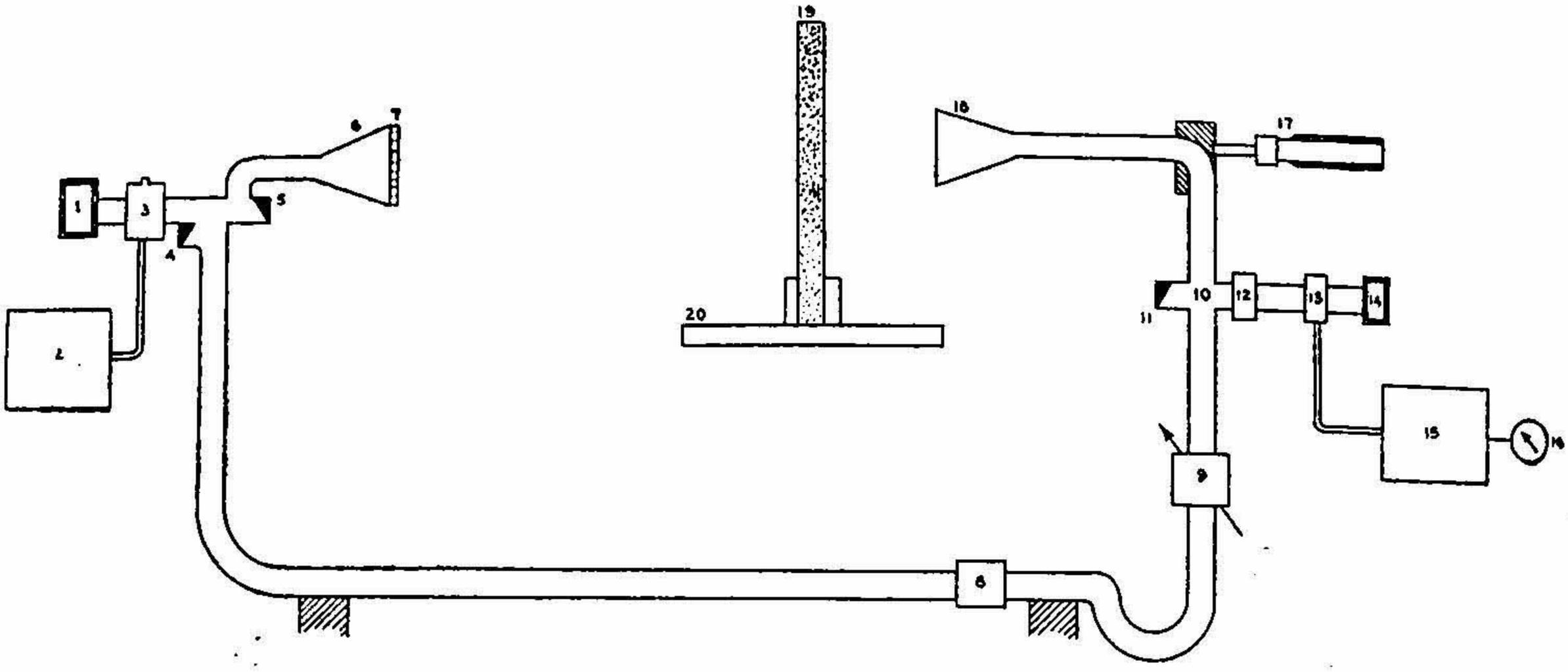

FIG. 2. Block schematic of the microwave interferometer.

1. Tunable short
2. Regulated power supply with square wave modulator
3. 723 A/B Klystron
4 & 5. Directional couplers
6. Transmitting horn
7. Metal plate lens
8. Fixed attenuator (PRD type 160)
9. Variable attenuator (PRD type 185 A)
10. Magic-tee
11. Matched termination (PRD 114)
12. Wave guide tuner (PRD 302)
13. Crystal (IN 23)
14. Tunable short
15. Detector amplifier
16. Weston galvanometer (0–30 μ A)
17. Slow motion drive
18. Receiving horn
19. Dielectric sample
20. Platform for mounting the sample

the klystron. The stability of the power supply system is $\pm$ 0·05 volt in the 300 volts d.c. line.

The detector amplifier consists of six stages of amplification; a twin-tee network tuned to 1000 c.p.s. being placed in the fourth stage provides selective amplification at 1000 c.p.s. The output stage of the amplifier is connected to a bridge network containing two 1N34 crystals in two of its arms and a galvanometer as an indicating instrument. The operating gain of the amplifier is 85 db. The characteristics of the power supply unit and the detector amplifier are the same as reported in a recent paper by Chatterjee and others (1954).

MICROWAVE COMPONENTS

Sectoral Horn.—Considerable theoretical and experimental work on vertically polarised horns appeared in the literature. Since the H-plane sectoral horn is characterised by a field distribution which tapers to zero at the edge of the aperture, the radiation pattern in the horizontal plane

is relatively free of minor lobes. It is for this reason that the H-plane sectoral horn has been preferred.

In order to design a H-plane horn which would give optimum gain and minimum beam width and side-lobe level, the following relation (Chu and Barrow, 1939) has been used.

$$\phi = 2 \, arc \cos \frac{L}{L + \delta'} \tag{1}$$

where L and ϕ represent respectively the length and the flare angle of the horn, δ represents the maximum departure of the wave-front from the aperture plane. In order that the emergent wave-front may be plane it is essential that $\frac{2\pi\delta}{\lambda}$ should be very small. As

$$\frac{\delta}{\lambda} = L \frac{1 - \cos \phi/2}{\lambda} \tag{2}$$

a large 'phase-slip' may under certain circumstances reduce the amplitude of the main lobe. The value of δ should be such that the maximum phase-slip should be less than $\pi/2$. δ is usually chosen to lie between 0·1 to 0.4 free-space wavelength. The design data of the horn, taking $\delta = 1 \cdot 09$ cm. are $L = 31 \cdot 12$ cm. $\phi = 30°$, aperture = 18 cm. at the operating wavelength, $\lambda = 3 \cdot 2$ cm. The aperture has been kept small $\simeq 6\lambda$ in order to have optimum gain. The flare angle has been kept small in order that the higher order modes generated at the throat discontinuity may become rapidly evanescent, thus allowing only the TE_{10} mode to exist. At the horn mouth, however, the effect of higher order modes is not negligible, especially, in view of the sharp discontinuity created by the small aperture. The E-plane and the H-plane characteristics of the horn as determined experimentally are shown in Figs. 5. and 6 respectively. The experimental value of the gain of the horn measured by the conventional method is 17 db.

Phase Correcting Lens for the Transmitting Horn.—The emergent beam from a small horn of the above type (Fig. 4 *a*) will essentially have a spherical wave front. This amounts to a change in the effective angles of incidence. Moreover, due to the inverse-distance attenuation law, there will be a non-uniform distribution of amplitude through the sample. In order that the emergent wave from the horn has a plane wave front, the transmitting horn has been fitted with E-plane metal-plane lens as shown in Fig. 4 *a*. The design of the E-plane lens has been made by utilising the following relations (Kock, 1946).

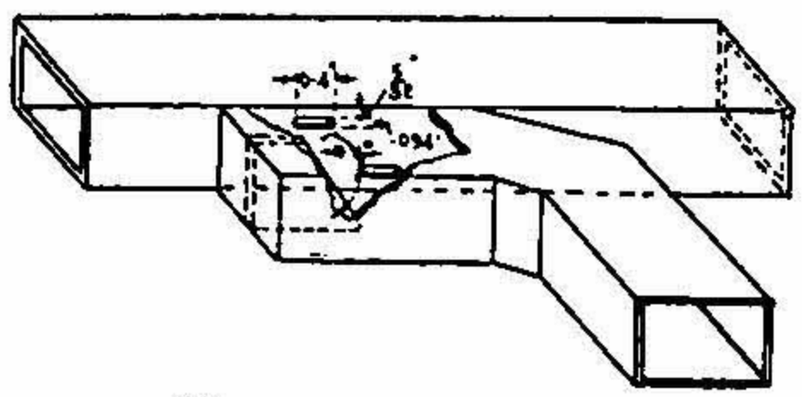

(c) BEAM DIVIDER

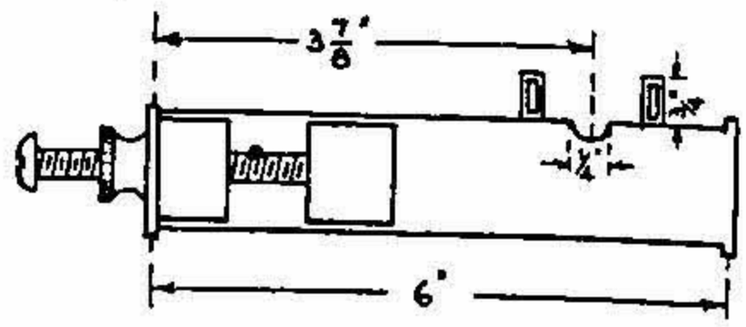

(e) KLYSTRON FEED SECTION

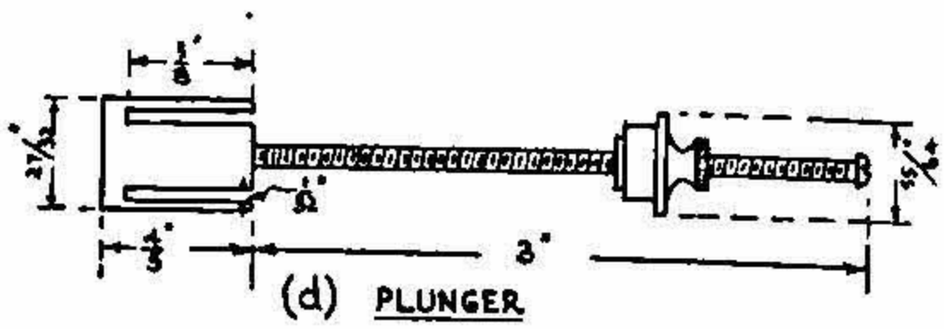

(d) PLUNGER

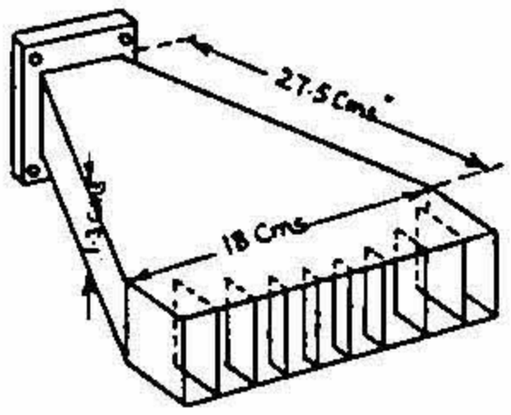

(a) HORN WITH LENS

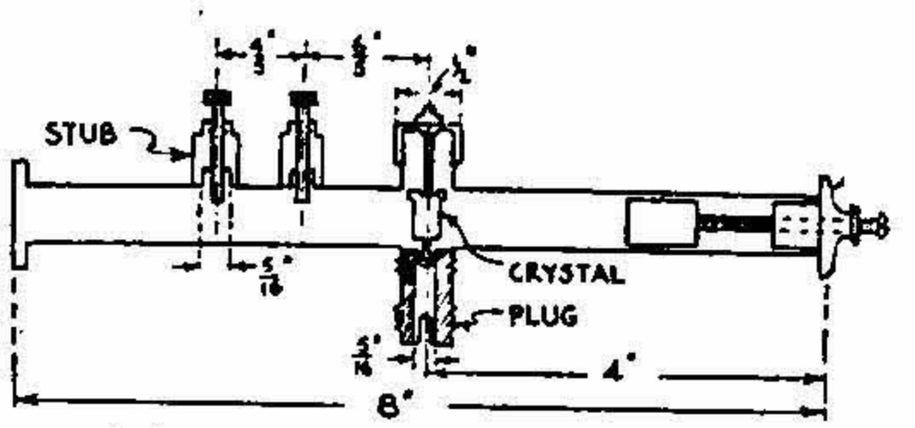

(b) DETECTING SECTION

FIG. 4. Dimensional sketches of some of the microwave components used for the construction of the interferometer.

$$\lambda_g = \frac{\lambda}{\left[1 - \left(\frac{\lambda}{2a}\right)^2\right]^{\frac{1}{2}}} \tag{3}$$

$$R = \frac{(1 - n)\,L}{1 - n\cos\phi/2} \tag{4}$$

$$n = \left[1 - \left(\frac{\lambda}{2a}\right)^2\right]^{\frac{1}{2}} \tag{5}$$

where R is the radius of curvature from the virtual apex to the tip of each parallel plate; a is the spacing between any two parallel plates; $a \geqslant \frac{\lambda}{2}$ so that the guide formed by parallel plates may not be opaque to the wave. n is the refractive index of the lens. The design data of the lens made from 1/64″ brass plates are as follows:—

Length of the plates from the axis to both the edges of the horn in cm.: 3·40, 2·30, 1·60, 1·00, 0·76, 0·76, 1·00, 1·60, 2·30, 3·40.

Spacing between any two plates $a = 2{\cdot}0$ cm.

Height of the plates parallel to the E vector $= 1{\cdot}30$ cm.

Refractive index of the lens $n = 0 \cdot 56$.

Wavelength in the guide formed by the lens $\lambda_g = 5 \cdot 37$ cm.

Frequency Sensitivity of the Lens.—At $\lambda < 3 \cdot 2$ cm., the aperture length increases in terms of wavelength, consequently, the loss in gain suffered due to phase slip is compensated. This results in practically uniform gain over a fairly wide band. The bandwidth B of a metal plate lens is given by the relation (Kraus, 1950).

$$B = \frac{2n\delta}{(1 - n^2)\, t'} \tag{6}$$

where δ is the tolerable path difference in free-space due to frequency shift of the microwave source and t is the thickness of the metal plate at the edge of the lens. Taking $\delta = 1 \cdot 09$ cm. and $t = 3 \cdot 11$ cm., $B \simeq 29\%$. The calculated bandwidth is rather high due to low value of t. The stability of the reflector voltage of 723 A/B is $\pm 0 \cdot 05$ volt. A variation of $\pm 0 \cdot 05$ volt changes the operating frequency by $\pm 0 \cdot 11$ mc./s. This frequency shift causes a change of $\pm 0 \cdot 000035$ cm. in the operating wavelength. So, the gain of the horn will remain fairly constant over this operating wavelength shift due to voltage fluctuation in the reflector of 723 A/B.

Tolerance of the Lens.—The degree of accuracy with which the lens should be constructed depends on the maximum irregularity that can be allowed in the wavefront. If the maximum irregularity due to either t or a is considered as $\lambda/16$, then allowing for the variations in both t and a the tolerances are (Kraus, 1950).

$$\Delta t = \pm \frac{0 \cdot 03}{1 - n} \tag{7}$$

$$\frac{\Delta a}{a} = \pm \frac{3n}{(1 - n^2)\, t} \% \tag{8}$$

For

$$n = 0 \cdot 56; \quad \lambda = 3 \cdot 2 \text{ cm.}; \quad \text{and } t = 3 \cdot 4 \text{ cm.}; \quad \Delta t = \pm 0 \cdot 22 \text{ cm.}$$

$$\Delta a = 1 \cdot 46\%$$

The characteristics of the horn fitted with the lens are shown in Figs. 5 and 6. It will be noticed that the half-power full-width of the directional characteristics in the E and the H-planes respectively are 50° and 15° without the lens as compared with 43° and 9° with the lens. It is also noticed that the H-plane characteristics are free of side lobes. A dimensional sketch of the horn with lens is shown in Fig. 4 *a*.

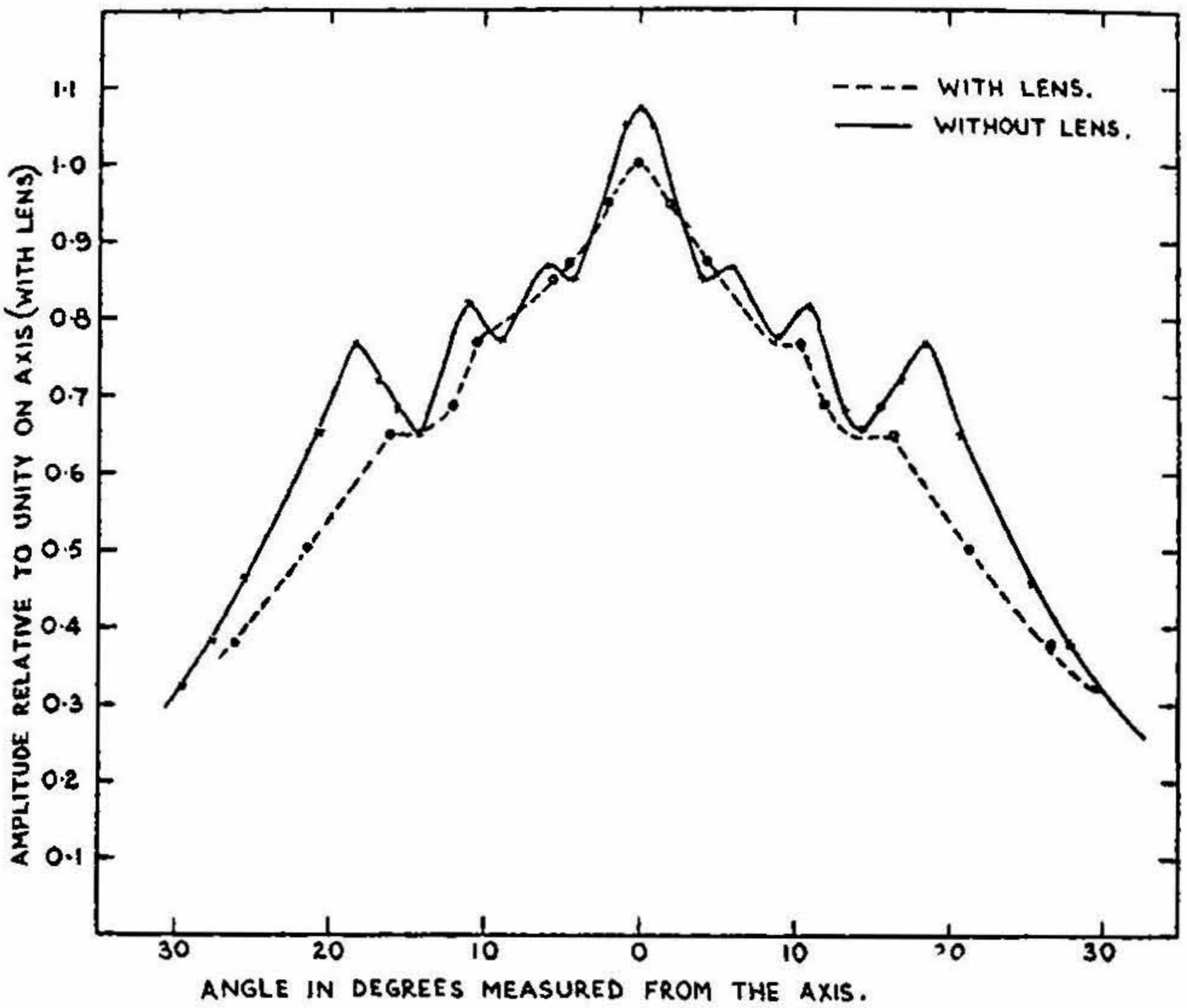

FIG. 5. Experimental radiation pattern of sectoral horn E-plane.

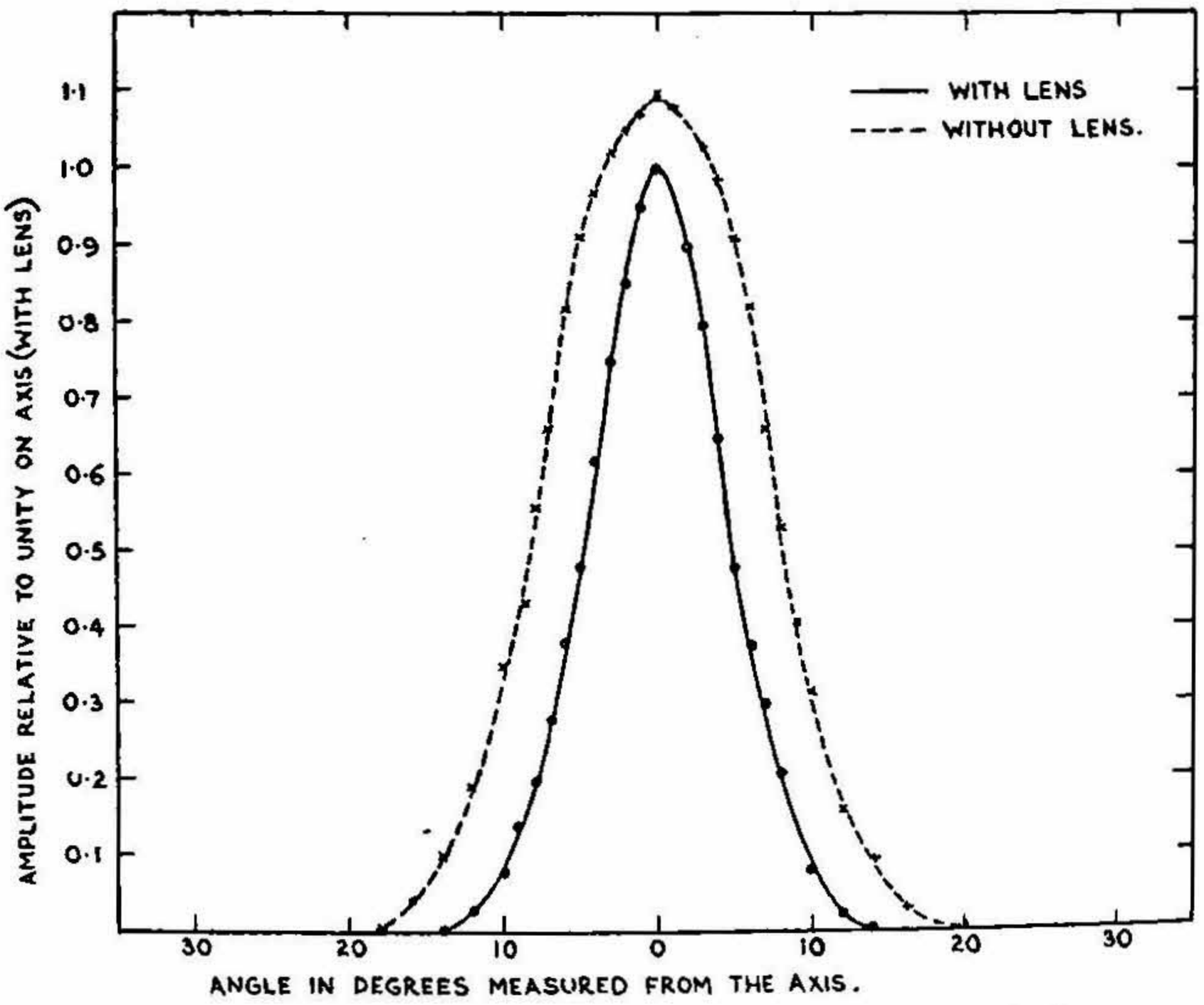

FIG. 6. Experimental radiation pattern of sectoral horn H-plane.

Klystron Feed.—The klystron is mounted directly on the broadface of a waveguide, so that the output probe of the klystron protrudes through a hole made at the centre of the broadface into the guide. This enables the excitation of the TE_{10} mode. One end of the guide is fitted with an adjustable plunger (Fig. 4 *d*). A dimensional sketch of the klystron feed is shown in Fig. 4 *e*.

Beam Divider.—The beam divider (4 *c*) consists of two waveguides of dimensions same as RG-51 U coupled together by means of two quarter wavelength slots staggered on the side wall of the primary guide. The terminating plate in the secondary arm consists of a fibre sheet on which soft iron particles are deposited. The variation of coupling with frequency as determined experimentally is shown in Fig. 7.

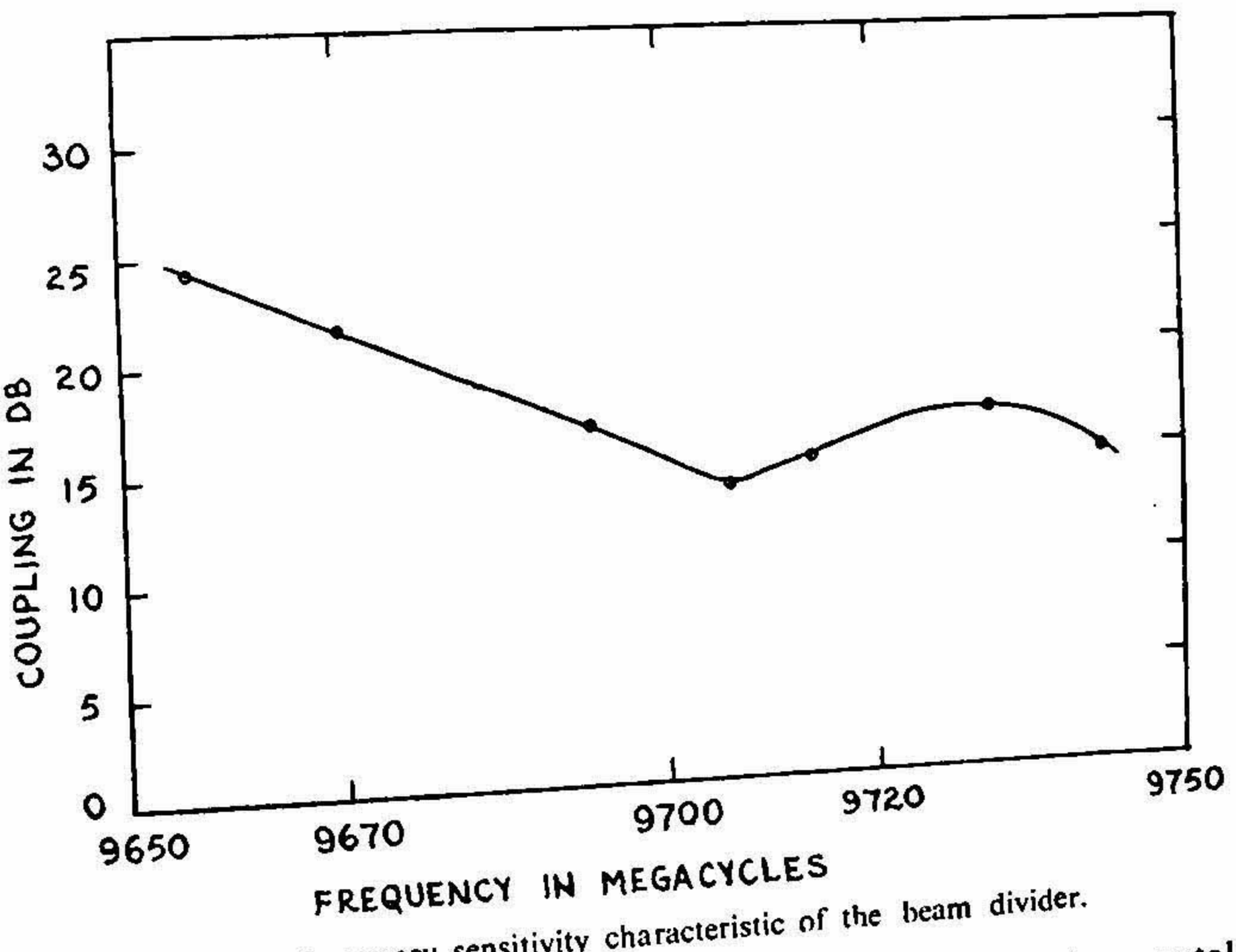

FIG. 7. Frequency sensitivity characteristic of the beam divider.

Detecting Section.—In the detecting section (Fig. 4 *b*), the crystal is mounted at the centre of the broadface directly across the waveguide and the output of the crystal is taken out by means of a coaxial adapter fitted to the waveguide. The matching of the detecting section is accomplished by means of a coarse and a fine adjustment. The coarse adjustment is done with a plunger provided with two quarter wave chokes, and fitted at one of the ends of the guide. The fine adjustment is done by two stubs placed quarter wavelength apart from each other and the crystal. The two stubs

project into the guide through two quarter wave chokes built concentrically with the stubs. A sketch of the plunger is given in Fig. 4 *d*.

MEASUREMENT OF DIELECTRIC CONSTANT OF SOME SOLID INSULATING MATERIALS WITH THE INTERFEROMETER

In order to test the performance of the interferometer, the dielectric constants of some solid insulating materials in the form of sheets have been measured. The theory of the method and the experimental results obtained are discussed below.

Theory of the Method.—When a plane electromagnetic wave of wavelength λ is incident normally on a dielectric sheet having dielectric constant ϵ and negligible loss ($\tan^2 \delta \approx 0$) situated in free space, the complex transmission coefficient of the material is given by the following relation (Montgomery. 1947).

$$Te^{-jt'} = \frac{4\sqrt{\epsilon}\, e^{-j\beta t}}{(\sqrt{\epsilon}+1)^2 - (\sqrt{\epsilon}-1)^2 e^{-2j\beta t}} \tag{9}$$

where t' is the phase change suffered by the wave in travelling through the material of thickness t. T represents the transmission coefficient of the sample. Separating the real and imaginary parts in (9), the following two equations are obtained.

$$(\sqrt{\epsilon}+1)^2 T \cos t' - (\sqrt{\epsilon}-1)^2 T \cos t' \cos 2\beta t + (\sqrt{\epsilon}-1)^2 T \sin t' \sin 2\beta t = 4\sqrt{\epsilon} \cos \beta t \tag{10}$$

$$(\sqrt{\epsilon}-1)^2 T \cos t' \sin 2\beta t - (\sqrt{\epsilon}+1)^2 T \sin t' + (\sqrt{\epsilon}-1)^2 T \sin t' \cos 2\beta t = 4\sqrt{\epsilon} \sin \beta t \tag{11}$$

As $\beta = \lambda/\sqrt{\epsilon}$ for the sample, the following relation is obtained from equations (10) and (11)

$$\cot t' = \frac{2\sqrt{\epsilon}}{1+\epsilon} \cot \frac{2\pi t}{\lambda}\sqrt{\epsilon} \tag{12}$$

In order to measure the phase shift, the position of the receiving horn is adjusted for null indication of the detector with and without the sample. The difference between the two positions of the receiving horn gives the phase Δ. The dielectric constant of the material placed in free space in terms of Δ is given by the following approximate relation

$$\epsilon = \left(1 + \frac{\Delta}{t}\right)^2 \tag{13}$$

The above equation is valid when t is large. In the free space technique of determining ϵ, t is restricted by practical considerations. So, ϵ given by (13) will be correct only when a correct value Δ_d is substituted in place of Δ. From (12) and (13) and neglecting the second order terms in Δ/t, the following expression is obtained.

$$\cot t' \simeq \cot \left(\frac{2\pi t}{\lambda}\sqrt{\epsilon}\right) \tag{14}$$

Using the measured value of Δ as Δ_m in (13) and substituting in (14) yields

$$\cot t' = -\tan\left[-\frac{2\pi t}{\lambda}\left(1+\frac{\Delta_m}{t}\right)+\frac{\pi}{2}\right] \tag{15}$$

Equation (13) gives

$$\Delta_d = t(\sqrt{\epsilon}-1) \tag{16}$$

From (12), (15) and (16)

$$\Delta_m - \Delta_d = \frac{\lambda}{4} - t\sqrt{\epsilon} - \frac{\lambda}{2\pi}\tan^{-1}\left[\frac{2\sqrt{\epsilon}}{1+\epsilon}\cot\frac{2\pi t\sqrt{\epsilon}}{\lambda}\right] \tag{17}$$

Variation of Shift with the Position of the Sample

The above theory for normal incidence does not take into account the effect of interaction taking place between the sample and the receiving horn and also between the air-sample and sample-air interfaces. The interaction between the sample-air interface and the receiving horn takes place due to the reflected ray from the sample reaching the horn. The interaction between the two interfaces of the sample takes place due to multiple reflections occurring within the sample. These interactions are responsible for making Δ dependent on the distance of the sample d from the receiving horn. The dependence of Δ on d by taking into account the interaction between the sample and the receiving horn is given by the following relation (Redheffer, 1949).

$$P = \frac{P_0 T^2}{1 - 2\rho R\cos\frac{4\pi d}{\lambda} + \rho^2 R^2}, \tag{18}$$

where P_0 is the power received by the horn in the absence of the dielectric sample and ρ represents an equivalent reflection coefficient of the receiving horn. The above relation shows that the received power and hence Δ will vary periodically with period $\lambda/2$ in d and with a nearly sinusoidal waveform. This is also borne out by the experimental results obtained (Fig. 8).

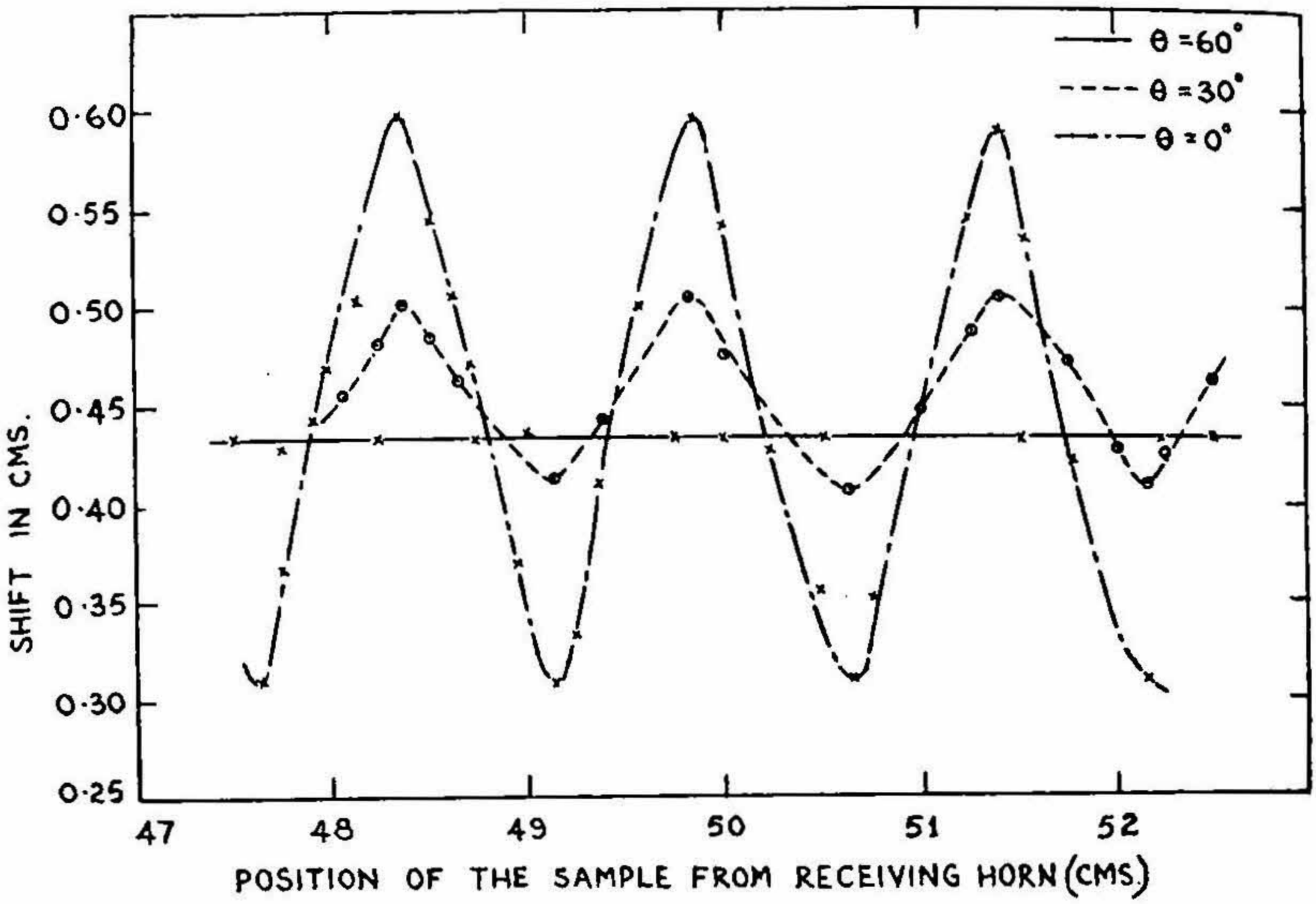

FIG. 8. Position of the sample from receiving horn *vs.* shift for various angles of incidence.

The effect of interaction can be reduced by allowing the wave to be incident at an angle other than the normal (0° with the vertical). When the angle of incidence corresponds to Brewster's angle, given by

$$\theta_B = \tan^{-1} \sqrt{\epsilon} \tag{19}$$

the reflected waves from the sample does not reach the receiver and Δ becomes independent of d, which is in agreement with the results obtained (Fig. 8). The angle at which Δ becomes independent of d differs for different materials. The values of θ_B as calculated from the experimental values of ϵ for different materials are given in Table II.

VARIATION OF SHIFT WITH ANGLES OF INCIDENCE

The variation of shift with different angles of incidence for a particular position of the sample (Perspex sheet) is shown in Fig. 9. The theoretical curve computed from the following relation is also shown for the sake of comparison

$$\frac{\Delta}{t} = -\cos\theta \pm \sqrt{\epsilon - \sin^2\theta} \tag{20}$$

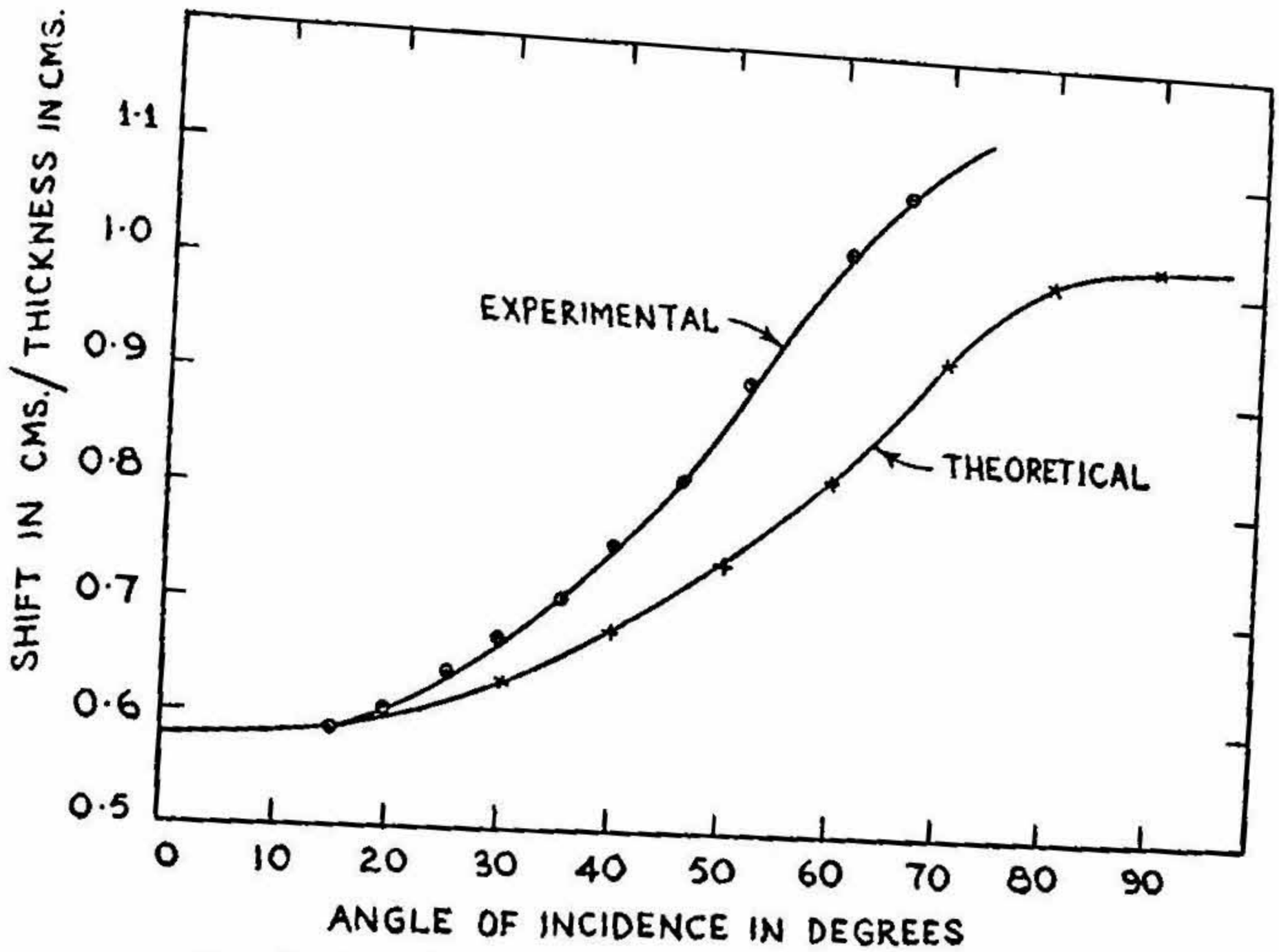

FIG. 9. Variation of shift with the angle of incidence.

EFFECT OF DIFFRACTION

The independence of Δ on d at Brewster's angle suggests a preference for determining ϵ when the sheet is arranged for arbitrary incidence. But arbitrary incidence changes the polarisation of the transmitted wave, as in this case the incident wave may be resolved into two components, one parallel and the other perpendicular to the polarisation of the receiving horn. Consequently, the transmitted wave is, in general, elliptically polarised for arbitrary incidence.

The effect of diffraction on shift at normal incidence has been studied experimentally (Fig. 10) by moving the sheet horizontally and vertically from the axis of the horns. The effect of diffraction has also been studied for different angles of incidence and the results for 0°, 30°, 40°, 57° are reported in Fig. 11. This study enables the determination of the minimum size of the sample necessary for determining ϵ by the present apparatus, so that the effect of diffraction would be minimum. It is noticed from Fig. 10 that the diffraction in the E-plane starts earlier as the dimension of the sample in the E-plane is less than that in the H-plane. It is also evident from Fig. 11 that the effect of diffraction increases and hence the size of the sample required is larger with increasing angles of incidence. Table III shows a comparative study of the minimum size of the sample required as determined

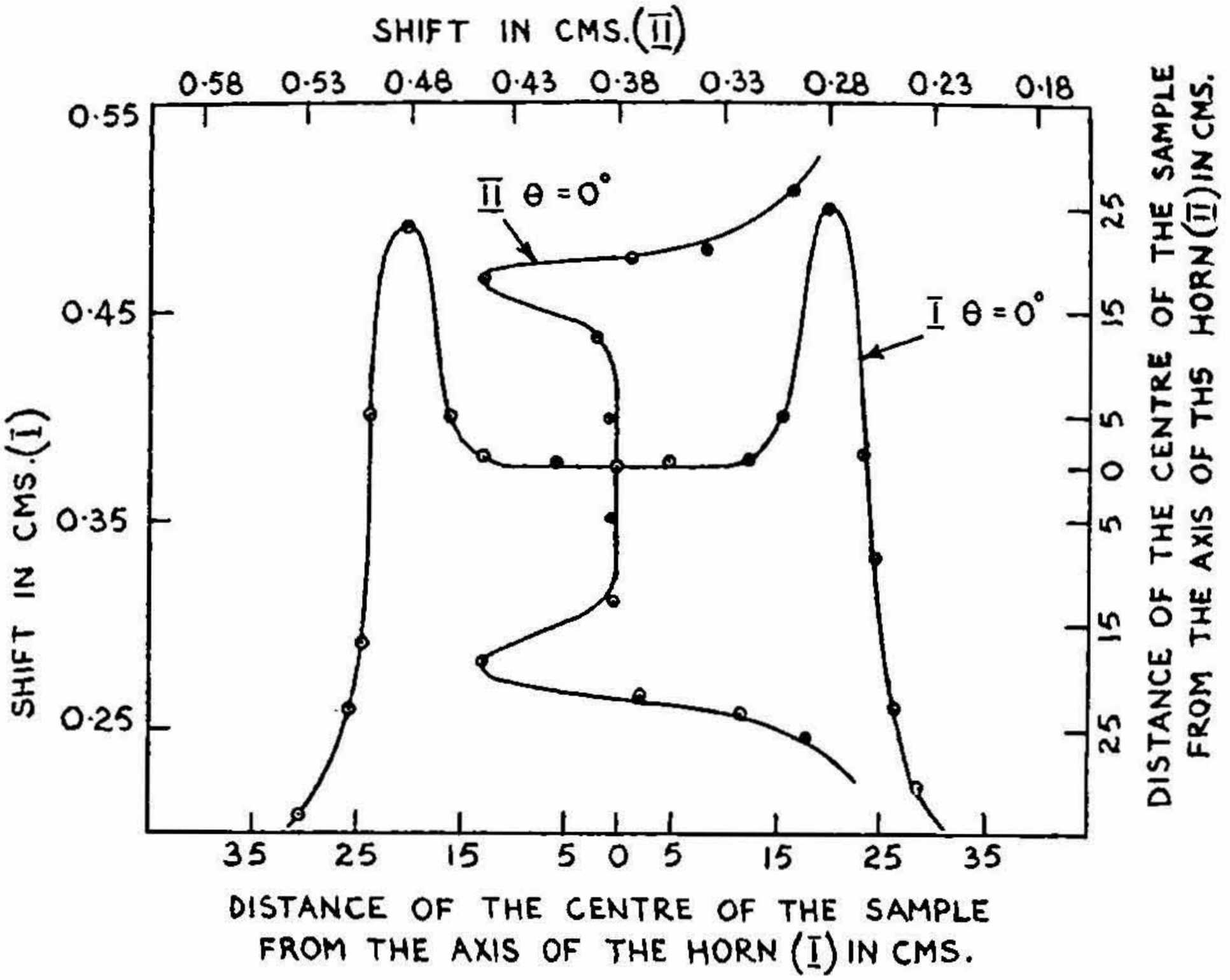

FIG. 10. Effect of diffraction for vertical and horizontal movement of the sample (Perspex).

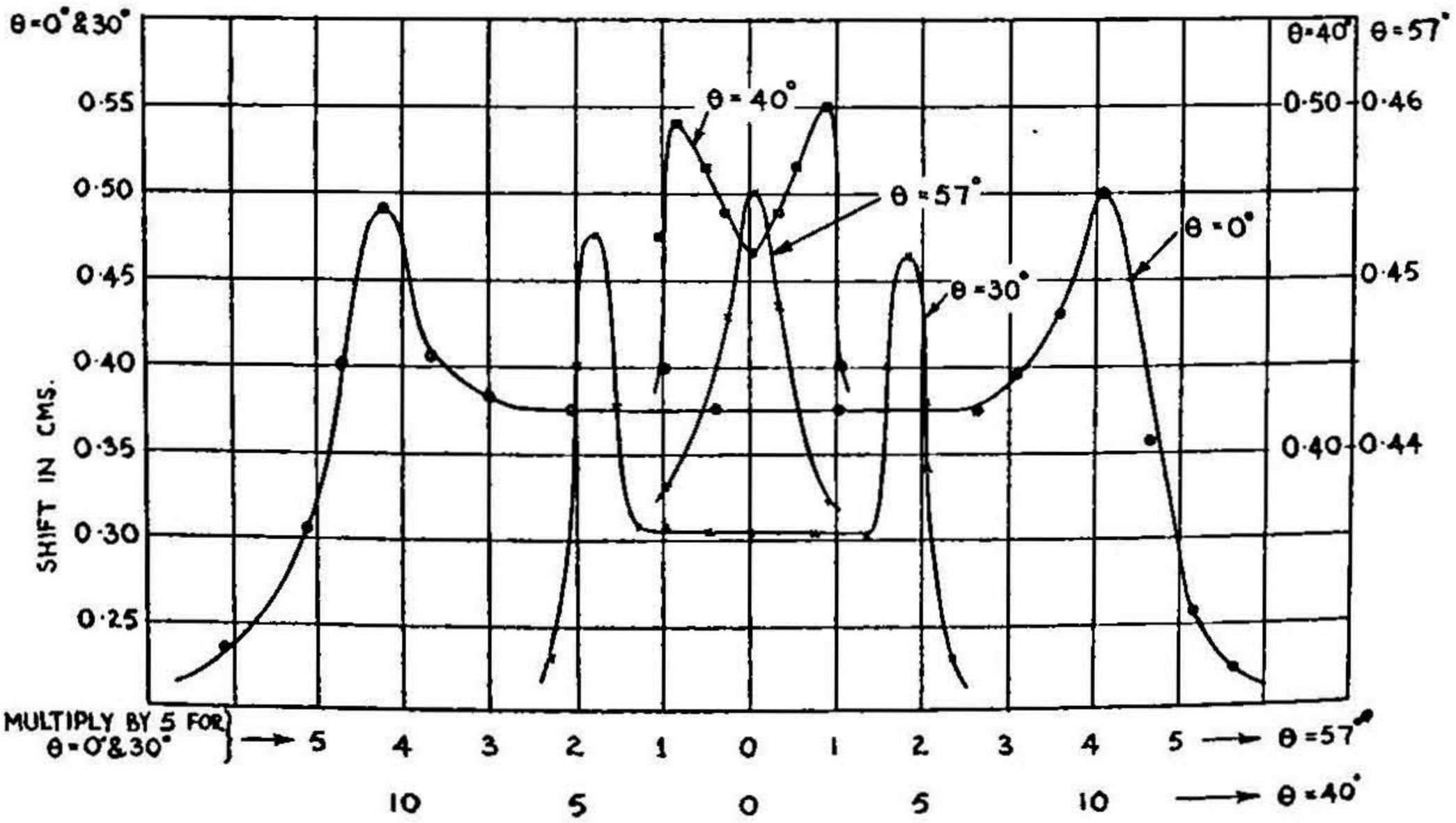

FIG. 11. Effect of diffraction at different angles of incidence.

experimentally and computed theoretically from the relation A sec θ where A indicates the size of the sample required at normal incidence.

The effect of diffraction at different angles of incidence when the sample is moved so that the centre of the sample is far away from the axis of the horn has been studied and the results for 0° and 35° are reported in Fig. 12.

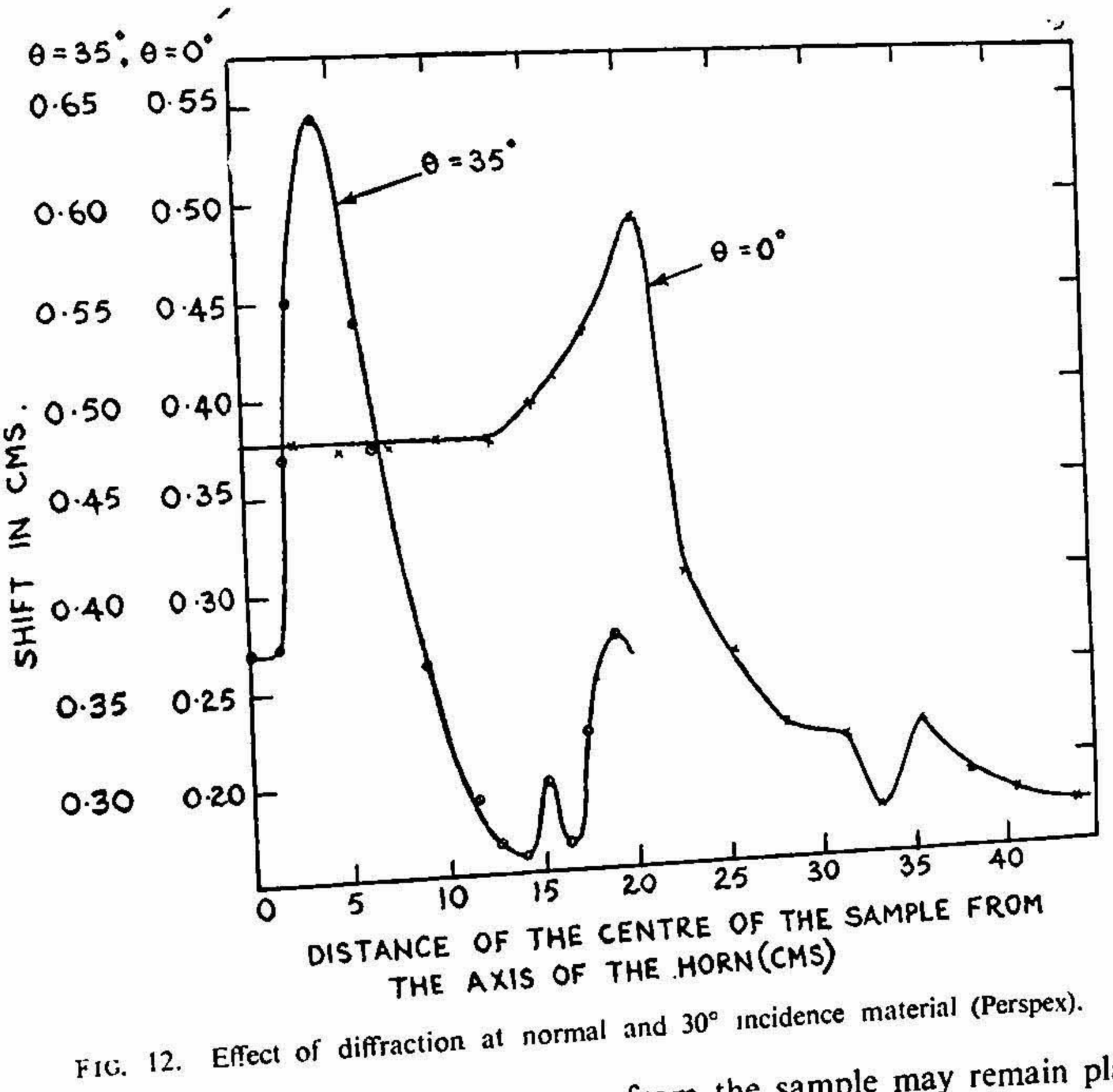

FIG. 12. Effect of diffraction at normal and 30° incidence material (Perspex).

In order that the transmitted wave from the sample may remain plane polarised as that of the receiving horn and also that the required size of the sample may be minimum, it is necessary to use normal incidence. In order to eliminate the effect of interaction, the phase shift has been measured in each case by placing the sample at distance d and $d + \lambda/4$ from the receiving horn and taking the shift as the average value of the two readings.

EXPERIMENTAL RESULTS

The results of measurement of ϵ for some solid insulating materials in the form of sheet are summarised in Table I. The shift is the average

TABLE I

Dielectric constant of some solid insulating materials at $\lambda = 3 \cdot 2$ cm. determined at normal incidence by the interferometer

Material	Sample size	Sample thickness in cm.	Shift in cm.	Values of ϵ	Values of ϵ corrected	Values of ϵ obtained by others
Perspex (Acrylic resin)	48″ × 36″	0·619	0·385	2·58	2·62	2·59 (1948) 2·71 (1950) Culshaw
Syndanyo ..	48″ × 36″	0·643	0·696	4·34	4·49	
		0·342	0·388	4·54	4·34	
Polyethylene ..	30″ × 29½″	0·623	0·310	2·24	2·29	2·24–2·31 (1948)
		1·247	0·625	2·25	2·15	
Bakelite ..	49″ × 25″	0·973	1·170	4·85	4·59	4·41–4·93 (1948)
Micanite ..	36″ × 24″	0·953	0·540	2·45	2·48	
Hard Asbestos ..	36″ × 33″	0·538	0·578	4·30	4·76	
Masonite ..	38″ × 25″	0·437	0·385	3·54	3·46	
Plywood ..	36″ × 36″	0·422	0·207	2·22	2·04	1·69 (1952)
Glass ..	45″ × 30″	0·634	0·578	3·65	4·12	4·00 (1952)

of values obtained when the sheet was placed at d and $d + \lambda/4$ from the receiving horn.

The Brewster's angles for different materials as calculated from the experimental values of ϵ are given in Table II.

TABLE II

Brewster's angles for different materials determined by the interferometer

Material	Perspex	Syndanyo	Polyethylene	Bakelite	Micanite
θ_B	58° 17′	64° 39′	56° 32′	64° 59′	57° 35′

Material	Hard Asbestos	Masonite	Plywood	Glass
θ_B	64° 23′	55° 44′	55° 1′	63° 47′

The minimum sizes of the sample (perspex) at 0°, 30°, 35°, etc., as determined from the diffraction experiments and calculated theoretically are given in Table III.

TABLE III

Theoretical and experimental values of the sizes of the sample (perspex)

(Dimensions are given for the H-plane only)

Angle	Experimental values	Theoretical values
0°	38″	44″
30°	43″	44″
35°	46″	46″
40	>48″	50″
57	>48″	70″

CONSISTENCY OF RESULTS

The accuracy with which ϵ can be measured depends on how accurately Δ and t can be measured. The accuracy of the measurement of Δ depends on the short-time and long-time stability of the system and also on the rate of change of the detector reading with the movement of the receiving horn at the minimum. The average of a large number of readings taken with one minute interval gives Δ within $\pm 0{\cdot}004$ cm. The average of a large number of readings spread out over several hours gives Δ within $\pm 0{\cdot}008$ cm. The response curves (Fig. 13) of the interferometer with and without the sample (perspex) show the sensitivity of the detector reading with respect to the position of the receiving horn. As the minima is rather flat but symmetrical, readings have been taken at 1 μa above the minima on both sides and the mean of the two readings is taken as the true position of the minima. At 1 μa above the minima, the rate of change of the detector reading is 1μa for 0·04 cm. movement of the horn, whereas at minima it is 0·08 cm. for 1 μa change. The noise level of the system at the operating gain is 1·0 μa. The change in the detector reading for different positions of the horn depends also on the linearity characteristics of the system which is shown in Fig. 14. The probable errors in Δ and t have been calculated from a large number of measurements in the case of each material and are given in Table IV. The difference between the measured and the desired value of Δ as calculated from Equation 17 for different materials is given in Table V.

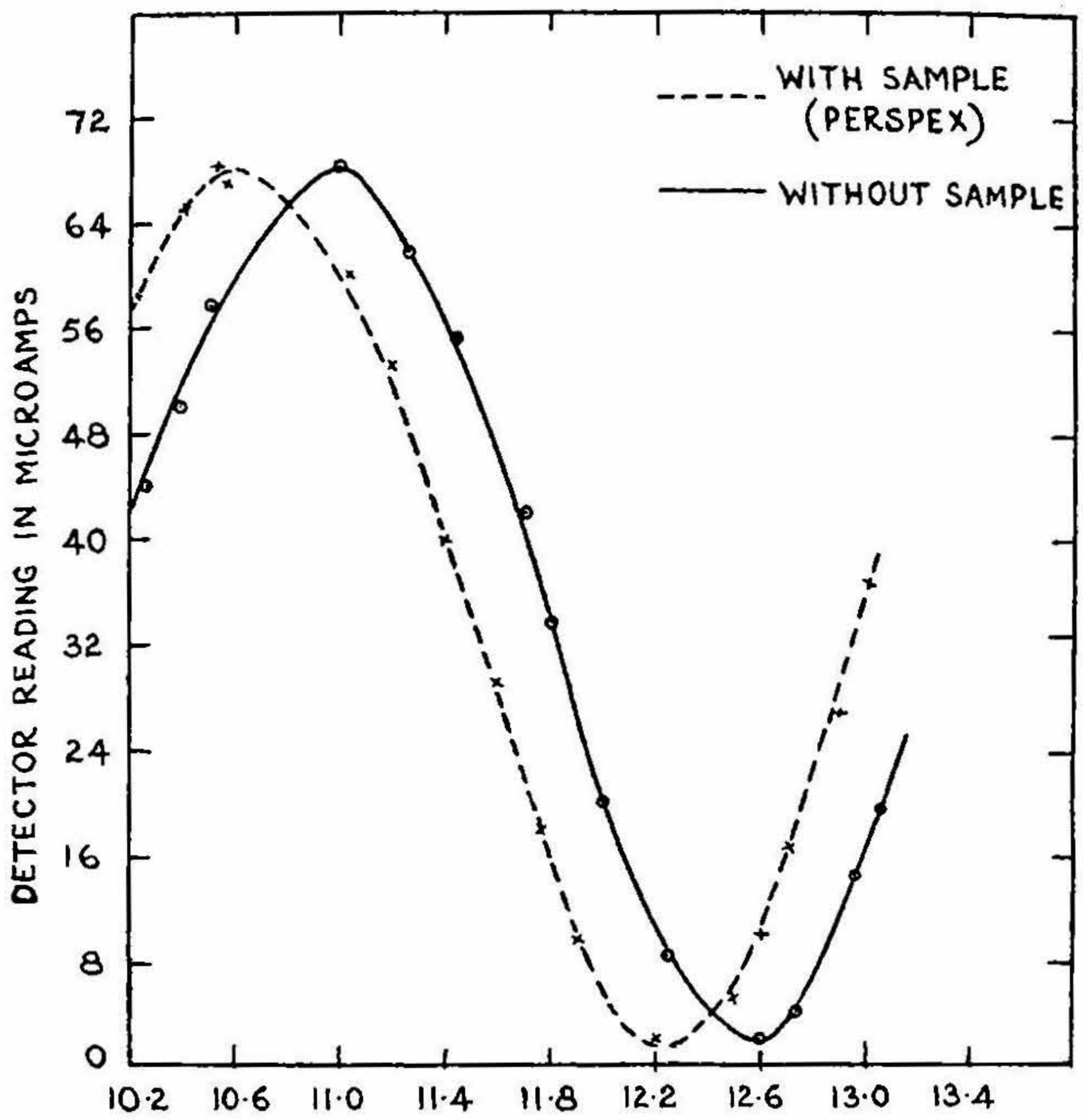

FIG. 13. Position of the receiving horn *vs.* detector reading with and without sample.

TABLE IV

Probable errors in Δ and t

Material	Error in Δ (cm.)	Error in t (cm.)
Perspex	±0·021	±0·006
Syndanyo	0·008	0·003
	0·010	0·007
Polyethylene ..	0·008	0·006
	0·010	0·010
Bakelite	0·021	0·002
Micanite	0·019	0·018
Hard Asbestos ..	0·024	0·008
Masonite	0·009	0·005
Plywood	0·013	0·004
Glass	0·014	<0·001

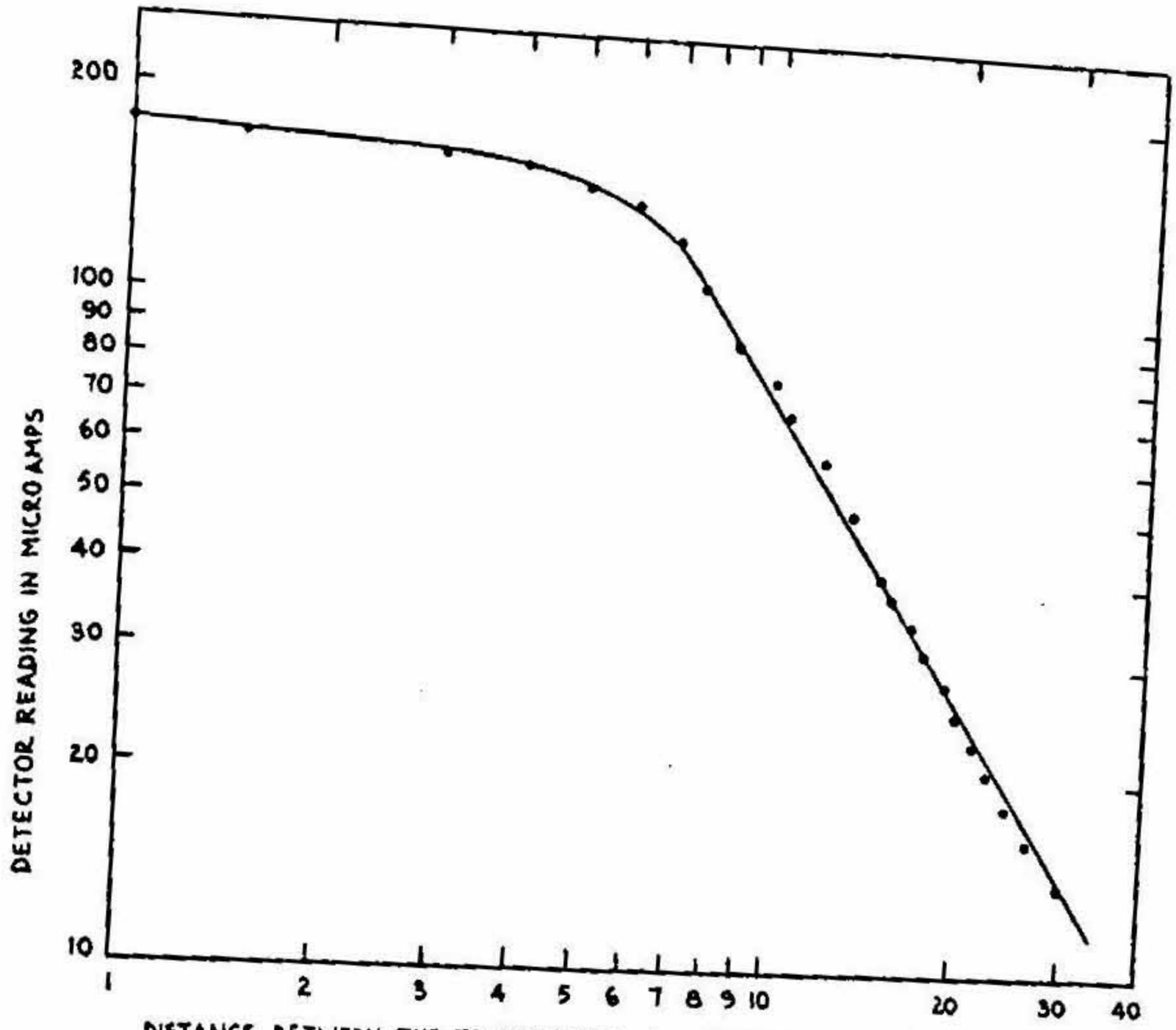

FIG. 14. Characteristic of the receiving system.

TABLE V

$\Delta_m - \Delta_d$ for different materials at normal incidence

Material	$\Delta_m - \Delta_d$
Perspex	−0·018
Syndanyo	−0·040
	+0·017
Polyethylene	−0·009
	+0·045
Bakelite	+0·058
Micanite	−0·008
Hard Asbestos	−0·058
Masonite	+0·008
Plywood	+0·026
Glass	−0·075

The comparatively high values or correction necessary to obtain the desired value of Δ in the case of glass, bakelite, asbestos is probably due to higher reflection coefficients of these materials.

The consistency of the results of a large number of measurements of Δ at normal incidence and at d and $d + \lambda/4$ and its effect on ϵ is shown in Table VI.

TABLE VI

Consistency in the measurement of ϵ at normal incidence

Material	Maximum values of Δ (cm.) obtained	Minimum values of Δ (cm.) obtained	Average deviation for all Δ values obtained	Maximum value of ϵ calculated from the approximate equation 13	Minimum value of ϵ from equation 13
Perspex ..	0·414	0·372	0·025	2·83	2·20
Syndanyo ..	0·713	0·680	0·009	4·25	4·24
	0·404	0·364	0·012	4·75	4·26
Polyethylene ..	0·319	0·292	0·009	2·33	2·16
	0·652	0·607	0·012	2·32	2·21
Bakelite ..	1·196	1·108	0·025	4·97	4·58
Micanite ..	0·572	0·502	0·022	2·54	2·35
Hard Asbestos	0·624	0·516	0·028	4·67	3·84
Masonite ..	0·409	0·355	0·010	3·74	3·28
Plywood ..	0·222	0·180	0·016	2·33	2·04
Glass ..	0·613	0·556	0·017	3·87	3·52

The consistency of the measurement of Δ and hence of ϵ for different angles of incidence is given in Table VII.

TABLE VII

Consistency in ϵ for different angles of incidence

(Material: Perspex. Computed from Fig. 8 and eq. 13)

Angle	Maximum value of Δ obtained	Minimum value of Δ obtained	Maximum value of ϵ obtained	Minimum value of ϵ obtained	Average deviation for ϵ
0° ..	0·600	0·308	3·88	2·24	0·825
30° ..	0·508	0·410	2·49	2·10	0·20
60° .. Sheet inclined towards the transmitting horn	0·438	0·428	2·73	2·68	0·02
60° .. Sheet inclined towards the receiving horn	0·438	0·426	2·73	2·67	0·03

The above table shows that as the angle of incidence approaches Brewster's angle, the average deviation becomes minimum.

Discussion

Size of the sample.—Fig. 10 shows that the diffraction in the E-plane starts earlier than that in the H-plane. This is probably due to the fact that the dimension of the sample in the E-plane is much less than that in the H-plane; the original size of the sample (perspex) being $48'' \times 36''$. Due to the non-availability of a square size sample, the theoretical and experimental values reported in Table III are for the dimensions in the H-plane only. Fig. 11 shows that diffraction starts at normal incidence and at 30° when the centre of the sample is away from the axis of the horn by 12·5 cm. and 6·25 cm. respectively. It is also noticed that in the case of 40° and higher angles of incidence, the diffraction effect is already present even when the centre of the sample is coincident with the axis of the horn. In other words, the size of the sample for 40° and higher angles of incidence should be greater than 48″. The single peak in the case of 57° incidence suggests that the effect of diffraction is very prominent and hence the minimum size of the sample required is much greater than 48″. The lower value of shift in the almost constant shift region in the case of 30° compared to that at normal incidence still remains to be explained.

Value of ϵ.—Tables I and VII show that the value of ϵ obtained for perspex at normal incidence agree within 1·5% with the value obtained at 60°. A more accurate value at 60° could be obtained by using a larger sample.

Limitations of the interferometer.—The sensitivity of the change in the detector reading with respect to the phase shift produced by the movement of the horn being low, the accuracy of the measurement is limited. In order to increase the sensitivity, a logarithmic amplifier is under construction.

A more accurate measurement of Δ requires a system having higher frequency stability. The construction of a Pound stabiliser is under progress for this purpose.

The experiment has been performed in a fairly big size room. In spite of this, the effect of random radiation scatter is present and no attempt has been made to eliminate the effect of stray reflections. The effect of random scatter affects the result more in the case of samples having higher reflection coefficients.

REFERENCES

Lengyel, B. A.	..	*Proc. I.R.E.*, 1949, **37**, 1242; *Electronics*, 1949 May, 164.
Culshaw, W.	..	*Pro. Phy. Soc.*, 1950, **63 B**, 939; *Ibid.*, 1953, **66**, 597.
Froome, K. D.	..	*Proc. Roy. Soc.*, 1954, **223 A**, 195; *Ibid.*, 1952, **213**, 123.
Artman, J. D.	..	*Rev. Sci. Inst.*, 1953, **24**, 873.
Chatterjee, S. K., Shenoy, P. R. and Rama Bai, C.		*J. Ind. Inst. Sci* , 1954, **36**, 107.
Chu, L. J. and Barrow, W. L.	..	*Trans. A.I.E.E.*, 1939, **58**, 333.
Kock, W. E.	..	*Proc. I.R.E.*, 1946, **34**, 828.
Kraus, J. D.	..	*Antennas*, 1950, 398–400, Published by McGraw-Hill Book Co.
Montgomery, C. G.	..	*Technique of Microwave Measurements*, 1947, 584, Published by McGraw-Hill Book Co.
Redheffer, A. M.	..	*Jour. Appl. Phys.*, 1949, **20**, 397.
Moreno, T.	..	*Microwave Transmission Design Data*, 1948, Published by McGraw-Hill Book Co.
Hull, G. F.	..	*Nuovo Cimento Supplemento*, 1952, No. 3, 288.

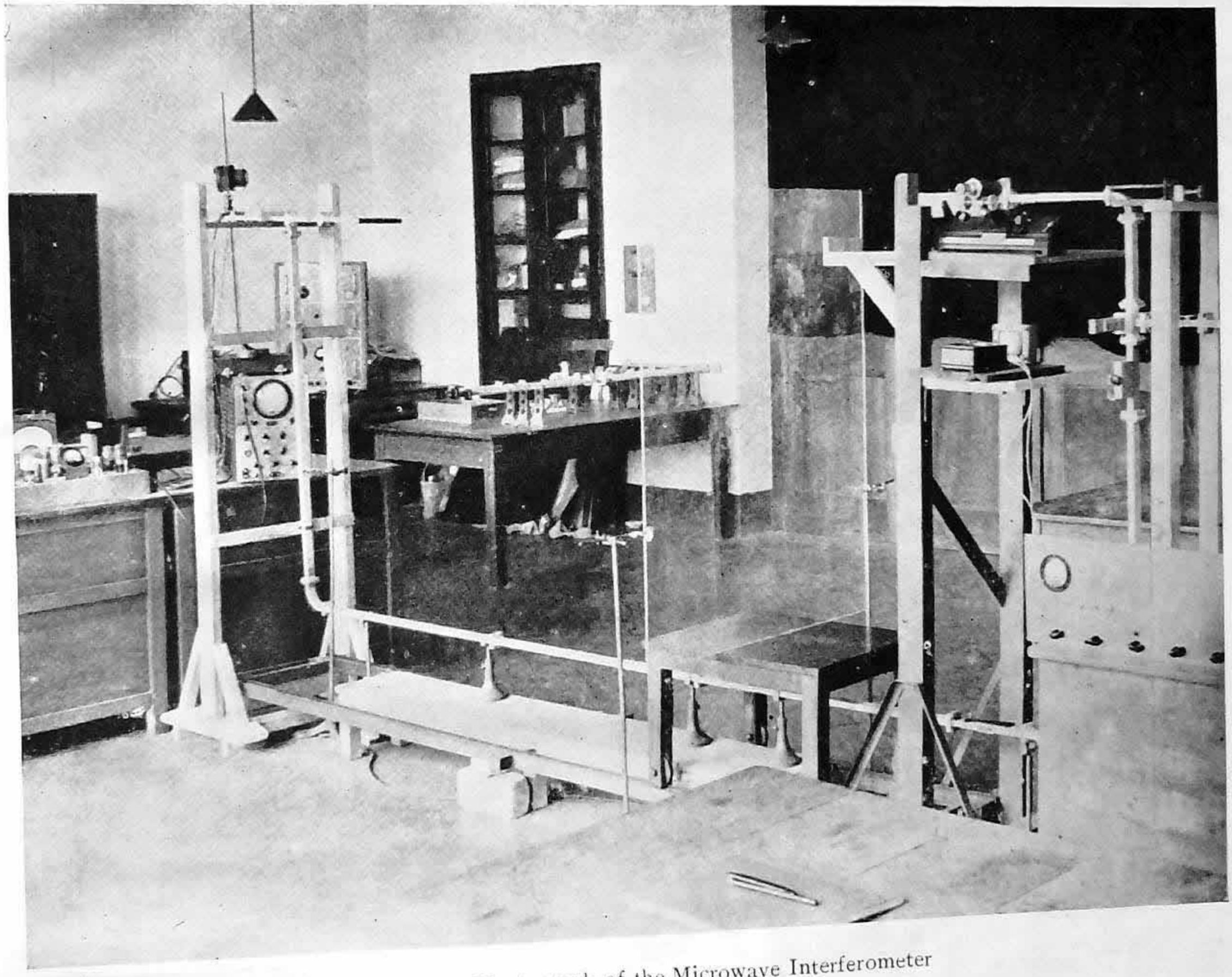

FIG. 1. Photograph of the Microwave Interferometer

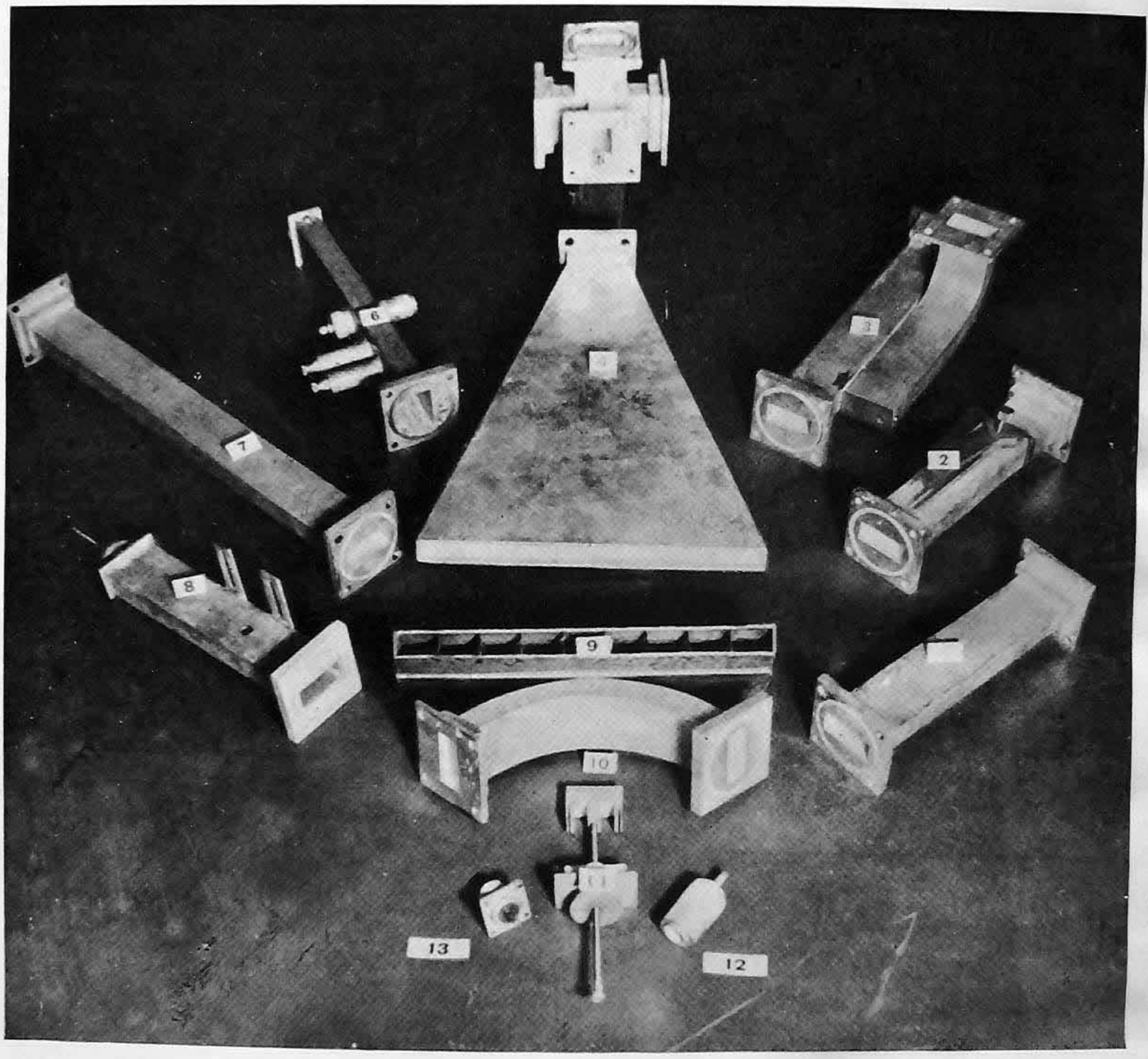

FIG. 3. Photograph of some Microwave components constructed for the Microwave Interferometer